J. Mech. Phys. Solids 155 (2021) 104572

Contents lists available at ScienceDirect

Journal of the Mechanics and Physics of Solids

journal homepage: www.elsevier.com/locate/jmps

Torsional and translational vibrations of a eukaryotic nucleus, and the prospect of vibrational mechanotransduction and therapy

Shaobao Liu [a,b,1], Haiqian Yang [c,1], Ming Wang [c,d], Jin Tian [c], Yuan Hong [c,d,e], Yuan Li [c,d], Guy M. Genin [c,d,e], Tian Jian Lu [a,b,*], Feng Xu [c,d,*]

[a] State Key Laboratory of Mechanics and Control of Mechanical Structures, Nanjing University of Aeronautics and Astronautics, Nanjing 210016, P. R. China
[b] MIIT Key Laboratory of Multifunctional Lightweight Materials and Structures, Nanjing University of Aeronautics, Nanjing, 210016, China
[c] Bioinspired Engineering and Biomechanics Center (BEBC), Xi'an Jiaotong University, Xi'an 710049, P.R. China
[d] MOE Key Laboratory of Biomedical Information Engineering, School of Life Science and Technology, Xi'an Jiaotong University, Xi'an 710049, P.R. China
[e] National Science Foundation Science and Technology Center for Engineering Mechanobiology, Washington University, St. Louis, MO 63130, USA

ARTICLE INFO

Keywords:
Cytoskeleton filament
Nuclear mechanotransduction
Mechanogenetics
Vibrational therapy
Oncotripsy

ABSTRACT

Certain eukaryotic cells are believed to sense and respond to vibrational stimuli that are too small even to be transduced by mechanosensitive ion channels. One possible mechanism of signal amplification and transduction is torsional and translational resonance of the nucleus, the stiffest and densest organelle in a eukaryotic cell. To explore this possibility, we developed a theoretical model that analyzes the natural frequencies of torsional and translational vibrations of the nucleus. The model predicts that the natural frequency for torsional vibration is dependent upon cytoskeletal contractility, while that for translational vibration is dependent upon cytoskeletal stiffness. Further analysis across many species and cell types suggests that, for most eukaryotic cells, torsional vibration is the dominant form of nuclear response to higher frequency stimuli, providing a new potential mechanism for frequency-based mechanotransduction.

1. Introduction

Although low-level vibration of the body has long been hypothesized in the mainstream mechanobiology and orthopedic literature to have therapeutic effects, the mechanisms underlying these effects are unknown, and their existence is a continued source of debate (Bacabac et al., 2006; Christiansen and Silva, 2006; Jing et al., 2017; Kim et al., 2012; Lynch et al., 2010; Tanaka et al., 2003; Turner et al., 1995). Some studies report that low-level vibration can take the place of exercise in certain ways (de Oliveira et al., 2019), but the literature has not reached consensus, and even amongst those who believe in these phenomena, reports of doses and frequency ranges that are efficacious are scattered and in conflict (Reynolds et al., 2018). Effects are reported at the level of individual cells in culture, with vibrational loading reported to affect viability and differentiation of stem cells (Edwards and Reilly, 2015; Tirkkonen et al., 2011), and at the level of multicellular systems, with lower-frequency vibrational loading possibly affecting human embryo development (Isachenko et al., 2011). Low intensity pulsed ultrasound may be a mechanism for a putative cancer therapy called

* Corresponding authors.
E-mail addresses: tjlu@nuaa.edu.cn (T.J. Lu), fengxu@mail.xjtu.edu.cn (F. Xu).
[1] Authors contributed equally

https://doi.org/10.1016/j.jmps.2021.104572
Received 17 March 2021; Received in revised form 7 June 2021; Accepted 15 July 2021
Available online 21 July 2021
0022-5096/© 2021 Elsevier Ltd. All rights reserved.

"sonodynamics" (Wood and Sehgal, 2015) or "oncotripsy" (Mittelstein et al., 2020; Schibber et al., 2019). Understanding the mechanisms underlying such treatments is critical for establishing and optimizing their efficacy.

A number of potential pathways have been tested in the search for sources of putative physiological or therapeutic benefits of vibration, but none has yet been supported definitively (Prisby et al., 2008; Wood and Sehgal, 2015). Pathways that have been rejected by the literature include paracrine signaling and enhanced transport (Lynch et al., 2011). Higher powered vibrations from ultrasound can open ion channels (Kubanek et al., 2016), permeabilize cell membranes (Deng et al., 2004), and modulate action potentials (Gavrilov et al., 1996; Pan et al., 2018). However, frequencies outside of the lower range of ultrasound (*e.g.*, shockwaves) are believed to be efficacious (Gamarra et al., 2010; Steinhauser and Schmidt, 2021; Wang et al., 2005), meaning that the phenomena that occur in ultrasound cannot fully explain reported effects of vibrations on cells. Membrane deformation is proposed as a mechanism of acoustic transduction in plants, but these require flexure of long, slender structures that are not present in the body (Liu et al., 2017; Peng et al., 2020; Tran et al., 2021). Thus, the search for possible mechanisms motivates detailed analysis of the vibrational responses of cells.

Others have developed simplified models of such responses by assuming the nucleus to be surrounded by isotropic cytoplasm (Heyden and Ortiz, 2016; Or and Kimmel, 2009; Schibber et al., 2019). However, in eukaryotic cells the nucleus connects to the cell membrane through a structured, fibrous cytoskeleton that is better approximated as having radially anisotropic or transversely isotropic initial stress and stiffness (Alisafaei et al., 2019; Qin et al., 2020). This has been established with some certainty for astrocytes (Wilhelmsson et al., 2006). A one-dimensional (1D) spring-mass-damper model has previously demonstrated the possibility that the relatively stiff and dense nucleus can vibrate within the cytoplasm, and estimated the natural frequency to be in the range of 10-1,000 Hz (Or and Kimmel, 2009). Further, a three-dimensional (3D) finite element model estimated the natural frequency of cell to be on the order of 0.1 MHz (Heyden and Ortiz, 2016) and the influence of viscoelasticity on resonant frequencies has also been investigated (Heyden and Ortiz, 2017). We developed a 3D analytical model capable of accounting for cytoskeletal contractility and anisotropy to identify the ranges of cellular responses (*i.e.*, torsional and translational vibrations of cell nuclei), which might be possible in response to mechanical stimuli and thereby establish targets for future experimentation testing the hypothesis that nuclear vibration is associated with transduction of vibrational signals by eukaryotic cells.

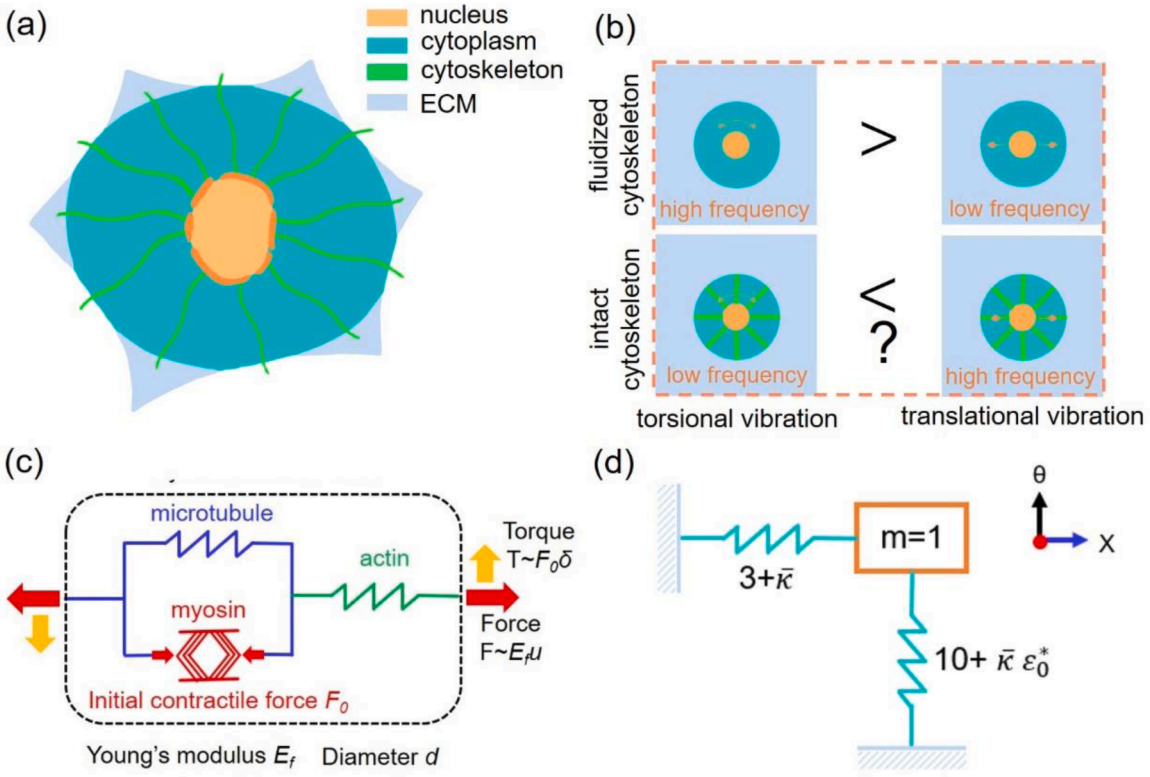

Figure 1. A model of translational and torsional vibrations of the cell nucleus under external stimuli. (a) Model of a eukaryotic cell within an effective extracellular matrix (ECM) environment that consists of neighboring cells and ECM proteins. (b) An objective is to determine the relative prevalence of torsional and translational vibrations. (c) Cytoskeletal filaments were modeled following published models in the literature (Alisafaei et al., 2019; Shakiba et al., 2020) as consisting of myosin with contractility F_0 in parallel with microtubules and in series with actin. Each of these filaments has effective Young's modulus E_f and diameter d. Our model reveals that the restoring force F as a result of the parallel displacement u due to the translation of the nucleus scales with the modulus E_f, while the restoring torque T as a result of the perpendicular displacement due to the torsion of the nucleus scales with the contractile force F_0. (d) The nucleus vibrates with two degrees of freedom, constrained by normalized translational stiffness $(3+\bar{\kappa})$ and normalized torsional stiffness $(10+\bar{\kappa}\varepsilon_0^*)$ for a nucleus with unit mass.

The nucleus typically presents as a spheroid or ellipsoid that is a few microns in diameter (Dundr and Misteli, 2001). Compared to the surrounding cytoplasm, the nucleus has greater mass density (Michelet-Habchi et al., 2005) and ten times greater stiffness(Caille et al., 2002), potentially enabling it to serve as a harmonic oscillator (Or and Kimmel, 2009; Schibber et al., 2019). We proposed that such stimulation of the nucleus and its environment are associated with substantial changes to cellular differentiation and gene expression (Uhler and Shivashankar, 2017; Wang and Tytell, 2009). By extending analysis of the model of Alisafaei, *et al.*, to account for vibration, we studied how the cytoskeleton interacts with a relatively rigid cell nucleus of an idealized cell, and how cytoskeletal tension and anisotropy govern the torsional and translational vibration of the nucleus (Fig. 1).

2. Methods

The fundamental (natural resonant) frequency corresponds to some peaks of the eigenfrequency spectrum, at which the amplitude of vibration is amplified. This frequency is an inherent property of a structure that depends on the structure's geometry and mechanical properties. We expect energy to be concentrated in the translational and rotational modes of the nucleus because of the mismatch in density and stiffness. We developed a theoretical model to analyze the modal shapes and natural frequencies of nuclear torsional and translational vibrations (Fig. 1b). As the elastic modulus of the nucleus (~5 kPa) is much larger than that of cytoplasm (~500 Pa) (Caille et al., 2002), the nucleus was considered as a rigid, linear inviscid sphere embedded in cytoplasm and extracellular matrix (ECM).

2.1. First-order Walpole model for a fluidized cytoskeleton

The simplest, baseline model was a combination of linear vibrational analysis and the Walpole solutions for translation and torsion of an ellipsoidal inclusion within an infinite, isotropic, linear solid (Walpole, 1991a,b). The cell cytoskeleton in this case would be fluidized, as can occur after rapid stretch (Krishnan et al., 2009; Lee et al., 2012; Nekouzadeh et al., 2008).

For a spherical nucleus with the radius r_n, the torsional vibration of nucleus follows the governing equation $I\ddot{\varphi} + K_t\delta = 0$, where $I = \frac{2}{5}mr_n{}^2$ is the moment of inertia and K_t is the effective resistance to torsional motion of nucleus. Walpole developed the theoretical solution for an infinitesimally rotated rigid ellipsoidal inclusion in an isotropic infinite elastic medium (Walpole, 1991b). For a sphere, the restoring moment for a small angular displacement δ is $T = -8\pi r_n{}^3 G\delta$. Thus, the torsional stiffness of nucleus is $K_t = \frac{dT}{d\varphi} = 8\pi r_n{}^3 G$, and the natural frequency for torsional vibration of nucleus is:

$$f_{tors} = \frac{1}{2\pi}\sqrt{\frac{K_t}{I}} = \sqrt{\frac{5}{\pi}\frac{Gr_n}{m}} \tag{1}$$

where m is the mass of nucleus, and G is the effective shear modulus of cytoplasm and ECM.

Translational vibration follows the governing equation $m\ddot{u} + Ku = 0$, where K is the effective translational stiffness. We applied Walpole's solution for the translation of a rigid ellipsoidal inclusion in an isotropic infinite elastic medium (Walpole, 1991a). For a sphere, the relation between the reaction force F of the medium surrounding the nucleus and the displacement u of the nucleus is $F = -6\pi Gr_n u$. This relation was applied to an analytical model of translational vibration of nucleus (Or and Kimmel, 2009). Thus, the translation stiffness of nucleus is $K = \frac{dF}{du} = 6\pi Gr_n$. Consequently, the natural frequency of translational vibration of nucleus yields

$$f_{tran} = \frac{1}{2\pi}\sqrt{\frac{K}{m}} = \sqrt{\frac{3}{2\pi}\frac{Gr_n}{m}} \tag{2}$$

2.2. Influence of the cytoskeleton

A more detailed solid mechanics approach was adopted to model the fibrous nature of the cytoskeleton. Following Alisafaei, *et al.* (Alisafaei et al., 2019), we considered a radially anisotropic cytoskeleton dominated by actomyosin contractile elements and microtubules (Fig. 1c). The nucleus is suspended by many well distributed cytoskeletal filaments (number N, Young's modulus E_f, diameter d and length l) embedded in an isotropic cytoplasm (shear modulus G_{cp}), with the distal ends of the cytoskeletal filaments affixed to the plasma membrane (Jean et al., 2005; Milner et al., 2012). For an individual fiber, by considering an infinitesimal translation of the nucleus (u) or a torsion angle of (δ), we found that the restoring force F scales with the modulus E_f, while the restoring torque T scales with the contractile force F_0 (Fig. 1(c)). We further extended this to a 3D model by considering a uniform distribution of filaments in all directions.

For torsional vibration, when the nucleus deviates from its equilibrium position with a small angular displacement (δ), each filament exerts a reaction torque on the nucleus that can be calculated as follows. The reaction force of this filament is

$$F = E_f A\varepsilon + F_o \tag{3}$$

where A is the cross-sectional area of each filament, ε is the strain of each filament, and F_o is the initial contractile force of each filament. From the law of cosines,

$$l'2 = (r_n + l)^2 + r_n{}^2 - 2r_n(r_n + l)\cos\delta \tag{4}$$

This gives

$$\varepsilon = \frac{l' - l}{l} = \frac{r_n(r_n + l)}{2l^2}\delta^2 \tag{5}$$

Thus, the reaction force is given by

$$F = E_f A \frac{r_n(r_n + l)}{2l^2}\delta^2 + F_o \tag{6}$$

The reaction torque on the nucleus from a single filament is

$$T_f = Fr_n \sin\left(\frac{r_n + l}{l}\delta\right) = -E_f A \frac{r_n(r_n + l)^2}{2l^3}\delta^3 - F_o \frac{r_n(r_n + l)}{l}\delta \tag{7}$$

We expect small angular displacements, $\delta^3 \ll \delta$, and thus simplify T_f as

$$T_f \approx -F_o \frac{r_n(r_n + l)}{l}\delta \tag{8}$$

As a result, the total moment provided by the cytoskeleton filaments is

$$\begin{aligned} T_f &= -F_o \frac{r_n(r_n + l)}{l}\delta \sum_{j=1}^{\left[\frac{\pi r_n}{\zeta}\right]} \sum_{i=1}^{\left[\frac{2\pi r_n \sin\theta}{\zeta}\right]} sin^2\left(j\frac{\zeta}{r_n}\right) \\ &\approx -F_o \frac{r_n(r_n + l)}{l}\delta \frac{N}{4\pi}\int_0^{2\pi}\int_0^{\pi} sin^3\theta d\theta d\varphi = -F_o \frac{r_n(r_n + l)}{l}\delta \frac{N}{4\pi} 2\pi \frac{4}{3} = -\frac{2}{3}NF_o \frac{r_n(r_n + l)}{l}\delta \end{aligned} \tag{9}$$

Thus, the torsional stiffness is modified as $K_t = 8\pi {r_n}^3 G + \frac{2N}{3}F_o\frac{r_n(r_n+l)}{l}$ and the natural frequency for nuclear torsional vibration is

$$f_{tors} = \frac{1}{2\pi}\sqrt{\frac{20\pi G r_n + \frac{5N}{3}F_o\frac{r_n + l}{r_n l}}{m}} \tag{10}$$

As for the translational vibration, when the nucleus deviates from its equilibrium position with a small translational displacement (u), every filament exerts a reaction force on the nucleus. The total reaction force of filaments along the displacement is

$$F_f = \frac{E_f' A}{l}\Delta l + F_o \tag{11}$$

where $\Delta l = ucos\theta$, E_f' is the effective Young's modulus of filaments, and d is the diameter of the filaments. The two ends of each individual filament are connected to the extracellular matrix and the nucleus, respectively, such that the effective Young's modulus of filaments E_f' is corrected by a factor ω through $E_f' = \omega E_f$. The correction factor can be calculated by (Liu et al., 2017; Lubarda, 2013)

$$\frac{1}{\omega} = \frac{E_f}{l}\left(\frac{(1 - v_{cm}{}^2)d}{E_{cm}} + \frac{l}{E_f} + \frac{(1 - v_{ne}{}^2)d}{E_{ne}}\right) \tag{12}$$

Projecting the force along the direction of u, we arrive at

$$F = -\frac{\omega E_f A}{l}ucos^2\theta - F_o cos\theta \tag{13}$$

Considering that the total effective number of filaments on the nucleus is N, the space between filaments could be estimated as $\zeta = \sqrt{\frac{4\pi}{N}}r_n$. Assuming that the filaments are uniformly distributed on the nuclear envelope, the total force on the nucleus is given by

$$\begin{aligned} F_f &= \sum_{j=0}^{\left[\frac{\pi r_n}{\zeta}\right]} \sum_{i=1}^{\left[\frac{2\pi r_n sin\theta}{\zeta}\right]} -\frac{\omega E_f A}{l}cos^2\theta u \\ &\approx -\frac{\omega E_f A}{l}u\frac{N}{4\pi}\int_0^{2\pi}\int_0^{\pi} cos^2\theta sin\theta d\theta d\varphi = -\frac{\omega E_f A}{l}u\frac{N}{4\pi}2\pi\int_0^{\pi}\left(sin\theta - sin^3\theta\right)d\theta = -\frac{\omega E_f A}{l}u\frac{N}{2}\left(2 - \frac{4}{3}\right) = -\frac{1}{3}N\frac{E_f' A}{l}u \end{aligned} \tag{14}$$

where $\theta = j\frac{\zeta}{r}$. $\frac{1}{3}NE_f A/l$ is the effective stiffness of cytoskeletal filaments. Thus, the translational stiffness is modified as $K = 6\pi G r_n +$

$\frac{1}{3}N\frac{E_f' A}{l}$ and the natural frequency of nuclear translational vibration is

$$f_{tran} = \frac{1}{2\pi}\sqrt{\frac{6\pi G r_n + \frac{1}{3}N\frac{E_f' A}{l}}{m}} \tag{15}$$

2.3. Influence of cell-cell interactions

Cell-cell interactions have long been known to affect mechanotransduction (Marquez et al., 2010; Wang et al., 2014). These interactions were modeled by varying the ratio of radius of nucleus to that of cell, $\eta = r_n/r_c$. For $\eta << 1$, the nucleus responds as if embedded in an infinitely large medium of cytoplasm. For larger η, the elastic resistance comes not only from deformation of the cytoplasm, but also from the ECM. In the latter case, the ECM affects the effective shear modulus of the medium within which the nucleus vibrates, and for a nucleus occupying the majority of the cell ($\eta \to 1$), the nucleus can be considered to be vibrating in ECM. The effective shear modulus surrounding the nucleus is linearized by

$$G = \left(1 - \frac{r_n}{r_c}\right)G_{cp} + \frac{r_n}{r_c}G_{ECM} \tag{16}$$

where G_{ECM} is the shear modulus of ECM.

For translational vibration, the effective Young's modulus of the cytoskeleton filaments E_f' is significantly influenced by ECM, which could be described by

$$\frac{1}{E_f'} = \frac{\pi d^2}{4l}\left(\frac{1}{k_{ECM}} + \frac{1}{k_f}\right) \tag{17}$$

where $k_f = \frac{\pi d^2}{4l}E_f$ is the stiffness of cytoskeleton filaments. The effective stiffness of ECM k_{ECM} was estimated by solving for the elastic field associated with exerting a uniform pressure on the semi-infinite elastic solid (Johnson, 1985; Love, 1929), which gives

$$k_{ECM} = \frac{\pi d E_{ECM}}{4(1 - \nu_{ECM}{}^2)} \tag{18}$$

where E_{ECM} is the Young's modulus of the ECM and ν_{ECM} is the its Poisson ratio.

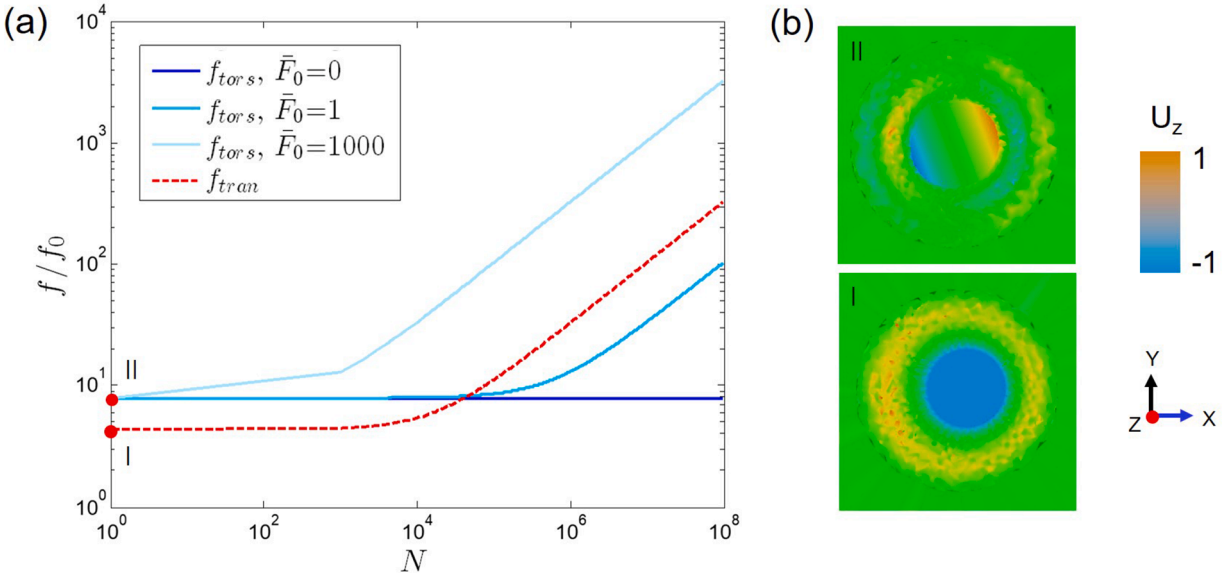

Figure 2. Effect of cytoskeletal filament density on natural frequency of nuclear vibration. (a) Normalized frequency f/f_0 of translational and torsional vibrations increases with the density of cytoskeleton filaments N for all levels of normalized contractility $\bar{F}_o$. The scale is characteristic frequency $f_0 = 3.12$ kHz. (b) Maximum normalized displacement in one direction of frequency analysis in a three-dimensional finite element simulation. The first order vibration of the cell nucleus is translational (I), while the second order vibration is torsional (II). f_{tors} and f_{tran} represent natural frequencies of torsional and translational vibrations, respectively. $\bar{F}_o$ is the dimensionless contractility of the cytoskeleton.

3. Results and discussion

The natural frequency of torsional vibration is dependent on cytoskeletal contractility, while that of translational vibration is dependent on cytoskeletal stiffness. Our models predict that torsional and vibrational oscillations of the nucleus depend strongly on cytoskeletal contraction and stiffness, and that the natural frequencies of these oscillations occur over a much broader range than earlier, simplified models predicted. With increasing numbers of cytoskeletal filaments, the fundamental frequency for torsional vibration increases provided that some cytoskeletal contractility is present (Fig. 2a). However, the fundamental frequency for translational vibration is independent of cytoskeletal contractility (Fig. 2a).

Closed form estimates are available for the case of cells with their cytoskeletons fluidized, as occurs following sufficient stretch, and for the case in which the nucleus is very small compared to the cell radius. For this case, $f_{tors} = \frac{1}{2\pi}\sqrt{\frac{20\pi G r_n}{m}} = \sqrt{20\pi} f_0$ and $f_{tran} = \frac{1}{2\pi}\sqrt{\frac{6\pi G r_n}{m}} = \sqrt{6\pi} f_0$, where $f_0 = \frac{1}{2\pi}\sqrt{\frac{G_{cp} r_n}{m}} = 3.12$ kHz is the characteristic frequency. This was confirmed by finite element modal analysis of a rigid sphere embedded in an infinite matrix (Fig. 2b). Thus, translational vibration occurs at a lower frequency under these circumstances. For baseline parameters (Table 1), this corresponds to $f_{tran} = 0.061$ MHz ($\sqrt{6\pi} f_0$), while the second order vibration is torsional vibration at a frequency of $f_{tors} = 0.112$ MHz ($\sqrt{20\pi} f_0$) (Fig. 2a), which is consistent with the response frequencies of cells to ultrasound (0.50-0.67 MHz) (Mittelstein et al., 2020).

These expressions and their extensions could be derived from Eqs. (10) and (15). The natural frequency of torsional vibration scales as:

$$f_{tors} = f_0\sqrt{20\pi(1-\eta+\eta\beta) + \frac{5N}{3}\pi\alpha^2\frac{1-\eta}{\eta^2}\overline{F}_o} \tag{19}$$

where $\alpha = \frac{d}{l}$ is the slenderness ratio of cytoskeletal filaments, $\beta = \frac{G_{ECM}}{G_{cp}}$ is the normalized shear modulus of the ECM, and $\overline{F}_o = \frac{F_o}{G_{cp}\pi d^2}$ is the dimensionless initial contractility of cytoskeleton filaments. This approaches $\sqrt{20\pi\beta} f_0$ for a relatively large nucleus (*i.e.*, $\eta \to 1$). $\overline{F}$

Table 1
Parameters used in the model of nucleus vibration

Parameter	Symbol	Value	Baseline
Density of nucleus	ρ	1.43×10^3 kg m^{-3} (Baddour et al., 2005)	1×10^3 kg m^{-3}
Young's modulus of cytoplasm	E_{cp}	500 Pa (Caille et al., 2002) 500 Pa (Or and Kimmel, 2009) 250 Pa (Barreto et al., 2013)	500 Pa
Poisson ratio of cytoplasm	ν_{cp}	0.49 (Barreto et al., 2013)	0.49
Shear modulus of cytoplasm	$G_{cp} = E_{cp}/[2(1+\nu_{cp})]$		160 Pa (calculated)
Poisson ratio of extracellular matrix	ν_{ECM}		0.3 (assumed)
Shear modulus of cytoplasm	$G_{ECM} = \mathrm{E}_{ECM}/[2(1+\nu_{ECM})]$		
Normalized shear modulus of extracellular matrix	$\beta = \frac{G_{ECM}}{G_{cp}}$		1 (assumed)
Young's modulus of cell nucleus	E_{cn}	1 kPa (Barreto et al., 2013)	rigid
Young's modulus of cytoskeleton filaments	E_f	2 GPa (microtubules) (Barreto et al., 2013) 2.60 GPa (Barreto et al., 2013) 1.20 GPa (microtubules) (Kardas et al., 2013)	1 GPa
Initial contractility	ρ_0	0.5 kPa (Alisafaei et al., 2019)	1 kPa
Number of cytoskeleton filaments	N	16,000 (Zeng et al., 2012)	16,000
Diameter of cytoskeleton filaments	d		10 nm
Radius of cell	r_c	15 μm (Zeng et al., 2012)	20 μm
Radius of nucleus	r_n	6.5 μm (Zeng et al., 2012)	10 μm
Mass of nucleus	$m = \frac{4}{3}\pi r_n^2\rho$		4.18×10^{-12}kg (calculated)
Characteristic frequency	$f_0 = \frac{1}{2\pi}\sqrt{\frac{G_{cp} r_n}{m}}$		3.12 kHz (calculated)
Length of cytoskeleton filaments	$l = r_c - r_n$	3.5-4 μm (Zeng et al., 2012)	10 μm
Slenderness ratio of cytoskeleton filament	$\alpha = \frac{d}{l}$		1×10^{-3} (calculated)
Initial contractile force of cytoskeleton filament	$F_o = \frac{4\pi r_n^2}{N}\rho_0$		7.8×10^{-11} N (calculated)
Initial strain due to initial Contractility of cytoskeleton filaments	$\varepsilon_o = \frac{F_o}{\pi d^2 \xi \mathrm{E}_f}$		
Dimensionless contractility of cytoskeleton filament	$\overline{F}_o = \frac{F_o}{G_{cp}\pi d^2}$		1.55×10^3 (calculated)

increases with increasing contractile force and decreases with increasing cytoskeletal stiffness. The natural frequency for torsional vibration increases as N increases (Fig. 2a).

The natural frequency of translational vibration of the nucleus scales as

$$f_{tran} = f_0\sqrt{6\pi(1-\eta+\eta\beta)+\frac{N\bar{k}_f}{12}\pi\alpha^2\frac{1-\eta}{\eta}} \tag{20}$$

where $\bar{k}_f = \frac{\xi E_f}{G_{cp}}$ is the dimensionless stiffness of a cytoskeletal filament, in which $\xi = \left(1+\alpha(1-\nu_{ECM}{}^2)\frac{E_f}{E_{ECM}}\right)^{-1}$ represents the influence of the ECM on the stiffness of cytoskeletal filaments. The natural frequency of nuclear torsional vibration approaches $\sqrt{6\pi\beta}f_0$ as the size of nucleus approaches that of the cell (*i.e.*, $\eta \to 1$) (Fig. 2a).

Comparing Eq. (19) with Eq. (20) leads to the conclusion that the natural frequency of torsional vibration is dependent on the dimensionless initial contractility ($\bar{F}_o$), while the translational vibration is dependent on the dimensionless cytoskeletal filament stiffness ($\bar{k}_f$).

Torsional vibration dominates the regime of higher frequency of cell nucleus vibration in most cells. Combining Eqs. (19) and (20), the ratio of natural frequency of torsional vibration to the natural frequency of linear vibration yields

$$\frac{f_{tors}}{f_{tran}} = \sqrt{\frac{10+\bar{\kappa}\epsilon_0^*}{3+\bar{\kappa}}} \tag{21}$$

where $\epsilon_0^* = 20\bar{F}_o/(\eta\bar{k}_f)$ is the initial strain due to initial contractility of cytoskeleton filaments, and $\bar{\kappa} = \frac{N}{24}\frac{\xi E_f}{G_{cp}}\alpha^2\frac{1-\eta}{\eta(1-\eta+\eta\beta)}$ is the dimensionless effective stiffness of the entire cytoskeleton. The Eq. (21) can be explained by that the nucleus vibrates in two degrees of freedom with the normalized translational stiffness ($3+\bar{\kappa}$) and normalized torsional stiffness ($10+\bar{\kappa}\epsilon_0^*$) for a nucleus with unit mass (Fig. 1d). With a fluidized cytoskeleton ($\bar{\kappa} \to 0$), the ratio of natural frequency of torsional vibration to that of translational vibration is $\sqrt{\frac{10}{3}}$, suggesting that the natural frequency of torsional vibration, in this special case, is in the same order as that of translational

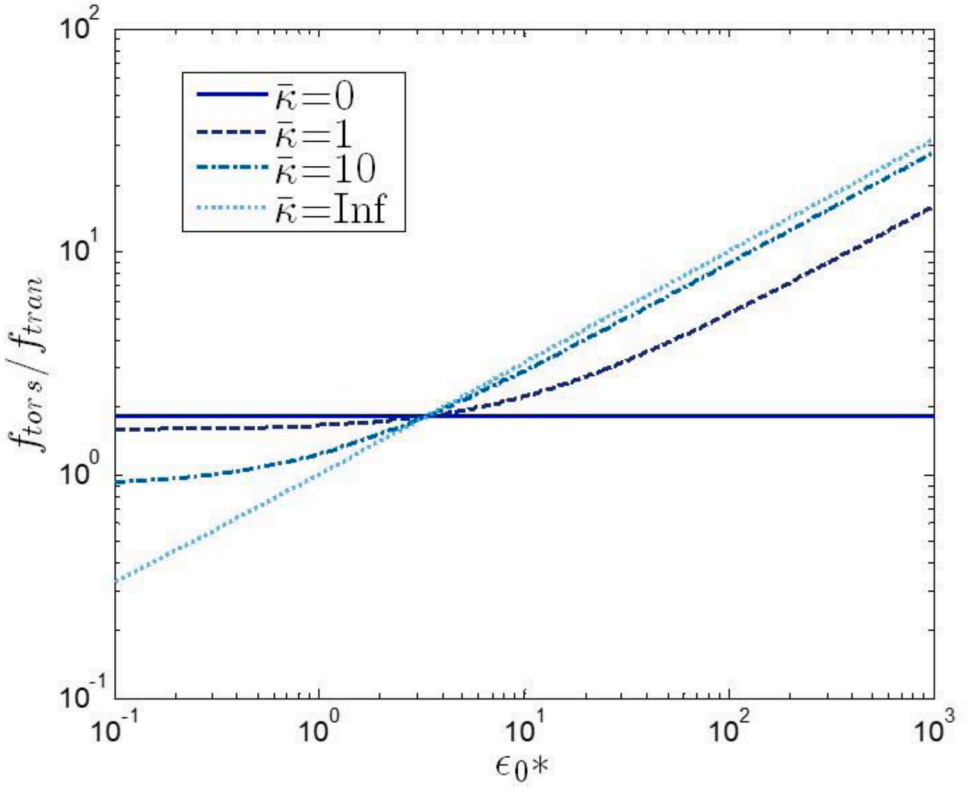

Figure 3. The ratio of natural frequency of torsional vibration to that of translational vibration increases with the initial strain for different dimensionless effective stiffness of cytoskeleton filaments $\bar{\kappa}$. The frequency ratio $\frac{f_{tors}}{f_{tran}}$ is between the two limits of $\sqrt{\frac{10}{3}}$ at $\bar{\kappa}=0$ and $\sqrt{\epsilon_0^*}$ at $\bar{\kappa}\to\infty$. There is a fixed point at $(\frac{10}{3}, \sqrt{\frac{10}{3}})$. f_{tors} and f_{tran} represent the natural frequencies of torsional and translational vibrations, respectively.

vibration.

The ratio of the natural frequency of torsional vibration to the translational vibration increases with the initial strain ε_0^* for different dimensionless effective cytoskeletal stiffness $\bar{\kappa}$ (Fig. 3). When filaments are much softer than the cytoplasm (*i.e.*, $\bar{\kappa} \ll 1$), the ratio $\frac{f_{tors}}{f_{tran}}$ approaches the isotropic solution $\sqrt{\frac{10}{3}}$, and when the filament is much stiffer than the cytoplasm (*i.e.*, $\bar{\kappa} \gg 1$), the ratio $\frac{f_{tors}}{f_{tran}}$ approaches the anisotropic solution $\sqrt{\varepsilon_0^*}$.

For the fundamental frequency of torsional vibration to be smaller than that of translational vibration, the following inequality must hold:

$$\bar{\kappa}\left(1-\varepsilon_0^*\right)\rangle 7 \tag{22}$$

This inequality indicates that torsional vibration dominates the lower frequency regime of vibrations of the cell nucleus (green region in Fig. 4). A smaller elastic modulus of the ECM results in a smaller natural frequency of both the translational and torsional vibrations. Animal cells typically have nuclei sized in half so that η is on the order of 0.5 (Table 2). For animal cells embedded in either soft ECM (~kPa) (*e.g.*, embryonic stem cells, neurons and neuronal stem cells, bone marrow stem cell, and lung cancer cells), or stiff ECM (~10 GPa) (*e.g.*, osteocyte, hematopoietic stem cell), the low frequency regime is governed by translational vibration while the high frequency regime is governed by torsional vibration. For intermediate ECM stiffness (~MPa) (*e.g.*, fibroblasts and, muscle stem cells), it is possible that the fundamental frequency of torsional vibration is smaller than that for translational vibration because equation Eq. (21) is non-monotonic with the respect to ECM stiffness. Liver cells are an exception, as they have relatively small nuclei ($\eta < 0.1$) and compliant ECM (~kPa), and can thus cross the phase boundary to the region of $\frac{f_{tors}}{f_{tran}} < 1$.

Plant cells typically have small nuclei (η<0.1). Cells within a stiff extracellular environment (~GPa), like pavement cells of *Arabidopsis thaliana*, respond to low frequency stimulation with translational vibration and to high frequency stimulation with torsional vibration. Cells within ECM of medium stiffness (~MPa), like bamboo cells and parenchymal cells (*e.g.*, potato cell, carrot cell and apple cell), are very close to the phase boundary like animal cells. Across a great many species and cell types, torsional vibration governs the high frequency regime while translational vibration governs the low frequency regime of nuclear response (Fig. 4).

Although therapeutic effects of vibration continue to be ambiguous, contradictory, and debated, these results provide a potential framework for experiment. What do these results mean for the many proposed mechanisms for vibrational therapy? The results in the paper do not support or refute any of the broad and contradictory literature on the topic. However, they do point to certain scaling laws that provide a framework for exploring these putative effects, and we conclude by outlining what the simple scaling relations derived here suggest.

First, if low amplitude vibrations are indeed transduced by cells in a meaningful way, and if the transduction likely occurs, as our arguments in the introduction suggest, on the interior of the cell, then the nucleus is likely involved because of the density mismatch

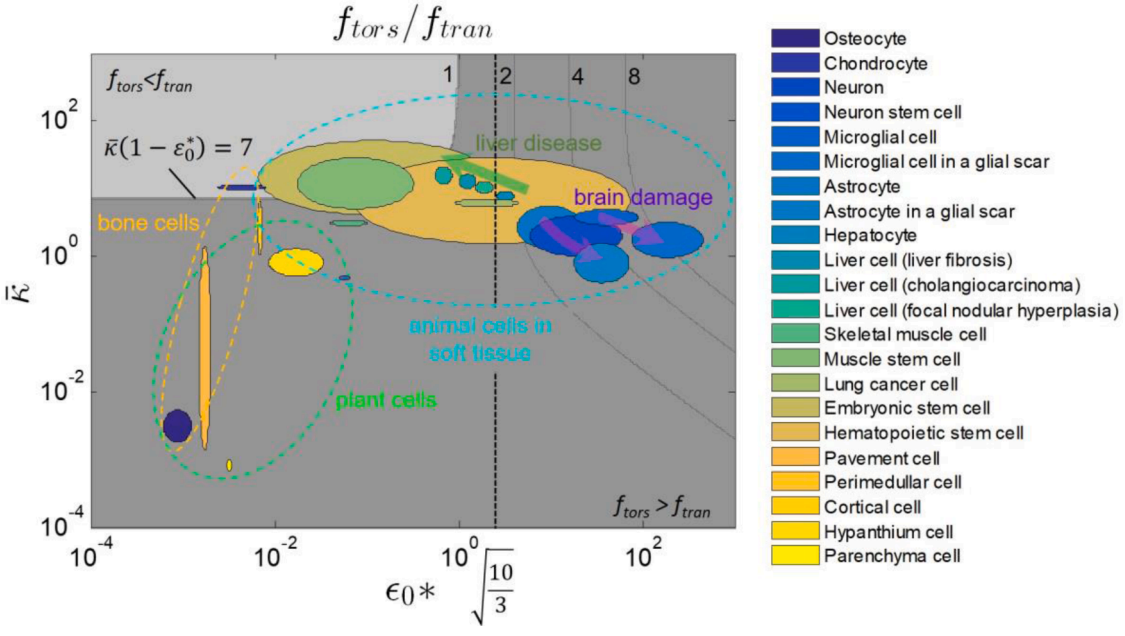

Figure 4. Natural frequency of torsional vibration versus translational vibration of the nucleus for a range of cell types. Torsional vibration dominates the regime of higher frequency (*i.e.*, $f_{tors} > f_{tran}$) for nuclear vibration in most cells, while torsional vibration dominates the regime of low frequency response (*i.e.*, $f_{tors} < f_{tran}$) of some types of cells (*e.g.*, chondrocytes and liver cells). The contour lines represent the frequency ratio $\frac{f_{tors}}{f_{tran}} = 1$, 2, 4, 8.

Table 2
Range of parameters for different cells

Tissue	Cell Type	r_n (μm)	r_c (μm)	E_{ECM} (Pa)
Bone	Osteocyte	2.50*	5.00-10.0 (Kleinnulend et al., 2012) #	1.04-1.48 $\times 10^{10}$(trabecular) (Rho et al., 1993) 1.86-2.07E$\times 10^{10}$ (cortical bone) (Rho et al., 1993)
Cartilage	Chondrocyte	~2.50 (Leipzig and Athanasiou, 2008) #	~4.00 (Leipzig and Athanasiou, 2008) #	0.40-1.18 $\times 10^{6}$ (superficial layer, Bovine articular cartilage) (Schinagl et al., 1997) 0.70-1.58$\times 10^{6}$ (ninth layer, Bovine articular cartilage) (Schinagl et al., 1997)
Brain	Neuron	7.00-10.00 (Sinnamon et al., 2012)	15.00 (Sinnamon et al., 2012)	0.100-1.00$\times 10^{3}$ (Tyler, 2012)
	Neuron stem cell	3.5*	7 (Saha et al., 2008) #	3.24$\times 10^{3}$ (Miller et al., 2000)
	Microglial cell	4 (Moshayedi et al., 2014) #	5 (Moshayedi et al., 2014) #	1.0-4.7$\times 10^{2}$ (Moeendarbary et al., 2017) 2.5-5.0$\times 10^{2}$ (Pogoda et al., 2014)
	Microglial cell in a glial scar	4 (Moshayedi et al., 2014) #	5 (Moshayedi et al., 2014) #	0.2-1.2$\times 10^{2}$ (Moeendarbary et al., 2017)
	Astrocyte	4 (Moshayedi et al., 2014) #	25 (Wilhelmsson et al., 2006)	1.0-4.7$\times 10^{2}$ (Moeendarbary et al., 2017) 2.5-5.0$\times 10^{2}$ (Pogoda et al., 2014)
	Astrocyte in a glial scar	4 (Moshayedi et al., 2014) #	25 (Wilhelmsson et al., 2006)	0.2-1.2$\times 10^{2}$ (Moeendarbary et al., 2017)
Liver	Hepatocyte	2.92-3.71 (Ranek et al., 1975)	10.85-14.85 (Darr and Hubel, 1997)	6.40$\times 10^{2}$ (Yeh et al., 2002)
	Liver cell (liver fibrosis)	2.92-3.71 (Ranek et al., 1975)	10.85-14.85 (Darr and Hubel, 1997)	1.65$\times 10^{3}$ (Yeh et al., 2002)
	Liver cell (cholangiocarcinoma)	2.92-3.71 (Ranek et al., 1975)	10.85-14.85 (Darr and Hubel, 1997)	3.00$\times 10^{3}$ (Yeh et al., 2002)
	Liver cell (focal nodular hyperplasia)	2.92-3.71 (Ranek et al., 1975)	10.85-14.85 (Darr and Hubel, 1997)	1.08$\times 10^{3}$ (Yeh et al., 2002)
Muscle	Skeletal muscle cell	10 (Swailes et al., 2006) #	20 (Swailes et al., 2006) #	1.00-3.00$\times 10^{5}$ (Munoz-Pinto et al., 2010)
	Muscle stem cell	3-6 (Muscle satellite cells) (Labarge and Blau, 2002) #	10-15 (Muscle satellite cells) (Labarge and Blau, 2002) #	0.896-1.11$\times 10^{5}$ (Cardiac muscle cells) (Anshu et al., 2001) 2.12-2.82$\times 10^{4}$ (Skeletal muscle cells) (Anshu et al., 2001)
Lungs	Lung cancer cell	5 (Kao et al., 2016) #	10 (Kao et al., 2016) #	1.00-5.00$\times 10^{3}$ (Yi et al., 2016)
Embryo	Embryonic stem cell	5-10 (Neural progenitors) (Reubinoff et al., 2001) † 3-6 (Adewumi et al., 2007)# 2-4 (Embryonic stem cell) (Paierowski et al., 2007) #	8-12 (Adewumi et al., 2007)#	10-200E+03(Embryonic chicken cardiocytes) (Anshu et al., 2001) 5-108E+03(microscale, embryonic tendon of chick) (Marturano et al., 2013) 7-21$\times 10^{3}$(microscale, embryonic tendon of chick) (Marturano et al., 2013)
Bone marrow	Hematopoietic stem cell	3-6 (Theise et al., 2003)# 3-4 μm (Paierowski et al., 2007) #	10-15 (Theise et al., 2003)#	0.025-2.47$\times 10^{4}$ (Jansen et al., 2015)
Leaf of *A. thaliana*	Pavement cell	2.00*	15.0-20.0 (Zhou et al., 2016)#	0.0035-3.50$\times 10^{10}$ (Liu et al., 2017)
Potato tuber	Perimedullar cell	10.6*	95-117 (Gibson, 2012)	3.60$\times 10^{6}$ (Gibson, 2012)
Carrot tap root	Cortical cell	3.6*	~36 (Gibson, 2012) #	2-14$\times 10^{6}$ (Gibson, 2012)
Apple hypanthium	Hypanthium cell	8*	19-82 (Liu et al., 2019)	2.8-5.8 $\times 10^{6}$ (Gibson, 2012)
Bamboo parenchyma	Parenchyma cell	2.5*	~25 (Dixon et al., 2017) #	3.5-4.0$\times 10^{10}$ (Gibson, 2012)

* Estimated value. The ratio of nuclear size to cell size is assumed to be 0.5 for animal and 0.1 for plant, respectively.
\# Measured value from the figures in references.
† In the calculation, the maximum radius of nucleus is taken to be the minimum radius of cell.

with the cytoplasm. Our results thus suggest that the first place to look is to search for motion of the nucleus relative to the cell membrane or cell wall.

Second, if such motion can be detected, it should undergo an increase of mode transformation frequency. At lower frequencies, torsional motions of the nucleus should dominate the vibrational responses of the cell. Translational motions should become evident as the frequency of excitation increases.

Third, if mechanotherapeutics do indeed work over prescribed frequency ranges, the search for mechanisms underlying these effects should involve the ways that torsional and translational vibrations trigger different mechanical signaling pathways. For instance, torsional vibration can generate shear stress on the nuclear envelope, while translational vibration can generate normal stresses.

Finally, the framework suggests ways that changes the mechanical microenvironments of cells can affect nuclear transduction of vibration. In diseases accompanied by softening or stiffening of the ECM (*e.g.*, cirrhosis of the liver and certain tumors), and in injury responses such as glial scarring, changes to the mechanical microenvironment can affect the fundamental frequencies and their ratios. For both microglial cells and astrocyte in glial scars, injury should result in the increase of frequency ratio of torsional vibration to translational vibration. Liver cell responses appear to change with disease and fibrosis so that the fundamental frequency of torsional vibration might drop even below that of translational vibration. Tuning mechanochemical microenvironmental factors such as ECM stiffness and cytoskeletal contractility can have substantial effect on vibrational response. This study provides a framework for exploring the possibility of frequency-based mechanotherapy, and possibly mechanogenetics.

4. Conclusion

By developing a theoretical model to characterize the torsional vibration and translational vibration of the nucleus, we identify a range of phenomena that can be used to assess the role of nuclear motion in putative therapeutic effects of low frequency vibration. Predictions show that the natural frequency of torsional vibration is dependent on initial cytoskeletal contractility, while translational vibration is dependent on the stiffness of the cytoskeleton. Torsional vibration dominates the high frequency regime of cell nucleus responses for most cells. Results suggest experiments to explore possible mechanisms of frequency-based cellular/nuclear mechanotransduction.

Declaration of competing interest

The authors declare that they have no known competing financial interests or personal relationships that could have appeared to influence the work reported in this paper.

Acknowledgement

This work was financially supported by the National Natural Science Foundation of China (11902155, 12032010, 11972280 and 11761161004), by the Natural Science Foundation of Jiangsu Province (BK20190382), by the foundation of Jiangsu Provincial Key Laboratory of Bionic Functional Materials, by the Foundation for the Priority Academic Program Development of Jiangsu Higher Education Institutions.

Author Statement

Shaobao Liu: Methodology, Software, Writing- Original draft preparation Software Haiqian Yang: Software, Writing- Original draft preparation Ming Wang: Data curation Jin Tian: Data curation Yuan Hong: Writing- Reviewing and Editing Yuan Li: Writing- Reviewing and Editing Guy M. Genin: Methodology, Writing- Reviewing and Editing Tian Jian Lu: Supervision, Funding acquisition Feng Xu: Conceptualization, Writing- Reviewing and Editing

References

Adewumi, O., Aflatoonian, B., Ahrlund-Richter, L., Amit, M., et al., 2007. Characterization of human embryonic stem cell lines by the International Stem Cell Initiative. Nat. Biotechnol. 25, 803–816.

Alisafaei, F., Jokhun, D.S., Shivashankar, G.V., Shenoy, V.B., 2019. Regulation of nuclear architecture, mechanics, and nucleocytoplasmic shuttling of epigenetic factors by cell geometric constraints endnote. P. Natl. Acad. Sci. USA 116, 13205.

Anshu, B.M., Amy, M.C., William, M.R., William, E.K., et al., 2001. Endothelial, cardiac muscle and skeletal muscle exhibit different viscous and elastic properties as determined by atomic force microscopy. J. Biomech. 34 (12), 1545–1553.

Bacabac, R.G., Smit, T.H., Van Loon, J.J., Doulabi, B.Z., et al., 2006. Bone cell responses to high-frequency vibration stress: does the nucleus oscillate within the cytoplasm? FASEB J 20, 858–864.

Baddour, R.E., Sherar, M.D., Hunt, J.W., Czarnota, G.J., et al., 2005. High-frequency ultrasound scattering from microspheres and single cells. J. Acoust. Soc. Am. 117, 934–943.

Barreto, S., Clausen, C.H., Perrault, C.M., Fletcher, D.A., et al., 2013. A multi-structural single cell model of force-induced interactions of cytoskeletal components. Biomaterials 34, 6119–6126.

Caille, N., Thoumine, O., Tardy, Y., Meister, J.J., 2002. Contribution of the nucleus to the mechanical properties of endothelial cells. J. Biomech. 35, 177–187.

Christiansen, B.A., Silva, M.J., 2006. The effect of varying magnitudes of whole-body vibration on several skeletal sites in mice. Ann. Biomed. Eng. 34, 1149–1156.

Darr, T., Hubel, A., 1997. Freezing characteristics of isolated pig and human hepatocytes. Cell Transplant 6, 173–183.

de Oliveira, L.C., de Oliveira, R.G., de Almeida Pires-Oliveira, D.A., 2019. Effects of whole-body vibration versus pilates exercise on bone mineral density in postmenopausal women: a randomized and controlled clinical trial. J. Geriatr. Phys. Ther. 42 (2), E23–E31.

Deng, C.X., Sieling, F., Pan, H., Cui, J.M., 2004. Ultrasound-induced cell membrane porosity. Ultrasound Med. Biol. 30 (4), 519–526.
Dixon, P.G., Muth, J.T., Xiao, X., Skylar-Scott, M.A., et al., 2017. 3D printed structures for modeling the Young's modulus of bamboo parenchyma. Acta Biomater, S1742706117308024.
Dundr, M., Misteli, T., 2001. Functional architecture in the cell nucleus. Biochem. J. 356 (Pt 2), 297–310.
Edwards, J.H., Reilly, G.C., 2015. Vibration stimuli and the differentiation of musculoskeletal progenitor cells: Review of results in vitro and in vivo. World J. Stem Cells 7, 568–582.
Gamarra, F., Spelsberg, F., Dellian, M., Goetz, A.E., 2010. Complete local tumor remission after therapy with extra-corporeally applied high-energy shock waves (HESW). Int. J. Cancer 55, 153–156.
Gavrilov, L.R., Tsirulnikov, E.M., Davies, I.A.I., 1996. Application of focused ultrasound for the stimulation of neural structures. Ultrasound Med. Biol. 22, 179–192.
Gibson, J.L., 2012. The hierarchical structure and mechanics of plant materials. J. R. Soc. Interface 9, 2749–2766.
Heyden, S, Ortiz, M., 2017. Investigation of the influence of viscoelasticity on oncotripsy. Comput. Method Appl. M 314, 314–322.
Heyden, S., Ortiz, M., 2016. Oncotripsy: targeting cancer cells selectively via resonant harmonic excitation. J. Mech. Phys. Solids 92, 164–175.
Isachenko, V., Maettner, R., Sterzik, K., Strehler, E., et al., 2011. In-vitro culture of human embryos with mechanical micro-vibration increases implantation rates. Reprod. Biomed. Online 22, 536–544.
Jansen, L.E., Birch, N.P., Schiffman, J.D., Crosby, A.J., et al., 2015. Mechanics of intact bone marrow. J. Mech. Behav. Biomed. 50, 299–307.
Jean, R.P., Chen, C.S., Spector, A.A., 2005. Finite-element analysis of the adhesion-cytoskeleton-nucleus mechanotransduction pathway during endothelial cell rounding: axisymmetric model. J. Biomech. Eng. 127, 594–600.
Jing, D., Yan, Z., Cai, J., Tong, S., et al., 2017. Low-1 level mechanical vibration improves bone microstructure, tissue mechanical properties and porous titanium implant osseointegration by promoting anabolic response in type 1 diabetic rabbits. Bone 11–21.
Johnson, K.L., 1985. Contact mechanics. J. Tribol. 108, 464.
Kao, Y.C., Jheng, J.R., Pan, H.J., Liao, W.Y., et al., 2016. Elevated hydrostatic pressure enhances the motility and enlarges the size of the lung cancer cells through aquaporin upregulation mediated by caveolin-1 and ERK1/2 signaling. Oncogene 36.
Kardas, D., Nackenhorst, U., Balzani, D., 2013. Computational model for the cell-mechanical response of the osteocyte cytoskeleton based on self-stabilizing tensegrity structures. Biomech. Model Mechanobiol. 12, 167–183.
Kim, I.S., Song, Y.M., Lee, B., Hwang, S.J., 2012. Human mesenchymal stromal cells are mechanosensitive to vibration stimuli. J. Dent. Res. 91, 1135.
Kleinnulend, J., Bacabac, R.G., Bakker, A.D., 2012. Mechanical loading and how it affects bone cells: the role of the osteocyte cytoskeleton in maintaining our skeleton. Eur. Cells. Mater. 24, 278–291.
Krishnan, R., Park, C.Y., Lin, Y.-C., Mead, J., et al., 2009. Reinforcement versus fluidization in cytoskeletal mechanoresponsiveness. PLoS One 4, e5486.
Kubanek, J., Shi, J., Marsh, J., Chen, D., et al., 2016. Ultrasound modulates ion channel currents. Sci. Rep. 6, 24170.
Labarge, M.A., Blau, H.M., 2002. Biological progression from adult bone marrow to mononucleate muscle stem cell to multinucleate muscle fiber in response to injury. Cell 111, 589–601.
Lee, S.L., Nekouzadeh, A., Butler, B., Pryse, K.M., et al., 2012. Physically-induced cytoskeleton remodeling of cells in three-dimensional culture. PLoS One 7, e45512.
Leipzig, N.D., Athanasiou, K.A., 2008. Static compression of single chondrocytes catabolically modifies single-cell gene expression. Biophys J 94, 2412–2422.
Liu, S., Jiao, J., Lu, T.J., Xu, F., et al., 2017. Arabidopsis leaf trichomes as acoustic antennae. Biophys J 113, 2068–2076.
Liu, S., Yang, H., Bian, Z., Tao, R., et al., 2019. Regulation on mechanical properties of spherically cellular fruits under osmotic stress. J. Mech. Phys. Solids 127, 182–190.
Love, A.E.H., 1929. The stress produced in a semi-infinite solid by pressure on part of the boundary. Philos. T. R. Soc. A 228, 377–420.
Lubarda, V.A., 2013. Circular loads on the surface of a half-space: Displacement and stress discontinuities under the load. Int. J. Solids Struct. 50, 1–14.
Lynch, M.A., Brodt, M.D., Silva, M.J., 2010. Skeletal effects of whole-body vibration in adult and aged mice. J. Orthop. Res. 28, 241–247.
Lynch, M.A., Brodt, M.D., Stephens, A.L., Civitelli, R., et al., 2011. Low-magnitude whole-body vibration does not enhance the anabolic skeletal effects of intermittent PTH in adult mice. J. Orthop. Res. 29, 465–472.
Marquez, J.P., Elson, E.L., Genin, G.M, 2010. Whole cell mechanics of contractile fibroblasts: relations between effective cellular and extracellular matrix moduli. Philos. T. R. Soc. A. 368.
Marturano, J.E., Arena, J.D., Schiller, Z.A., Georgakoudi, I., et al., 2013. Characterization of mechanical and biochemical properties of developing embryonic tendon. Proc. Natl. Acad. Sci. U.S.A. 110, 6370–6375.
Michelet-Habchi, C., Incerti, S., Aguer, P., Barberet, P., et al., 2005. 3D imaging of microscopic structures using a proton beam. IEEE T. Nucl. Sci. 52, 612–617.
Miller, K., Chinzei, K., Orssengo, G., Bednarz, P., 2000. Mechanical properties of brain tissue in-vivo: experiment and computer simulation. J. Biomech. 33, 1369–1376.
Milner, J.S., Grol, M.W., Beaucage, K.L., Dixon, S.J., et al., 2012. Finite-element modeling of viscoelastic cells during high-frequency cyclic strain. J. Funct. Biomater. 3, 209–224.
Mittelstein, D.R., Ye, J., Schibber, E.F., Roychoudhury, A., et al., 2020. Selective ablation of cancer cells with low intensity pulsed ultrasound. Appl. Phys. Lett. 116, 013701.
Moeendarbary, E., Weber, I.P., Sheridan, G.K., Koser, D.E., et al., 2017. The soft mechanical signature of glial scars in the central nervous system. Nat. Commun. 8, 14787.
Moshayedi, P., Ng, G., Kwok, J.C.F., Yeo, G.S.H., et al., 2014. The relationship between glial cell mechanosensitivity and foreign body reactions in the central nervous system. Biomaterials 35, 3919–3925.
Munoz-Pinto, D.J., Bulick, A.S., Hahn, M.S., 2010. Uncoupled investigation of scaffold modulus and mesh size on smooth muscle cell behavior. J. Biomed. Mater. Res. A 90A (1), 303–316.
Nekouzadeh, A., Pryse, K.M., Elson, E.L., Genin, G.M., 2008. Stretch-activated force shedding, force recovery, and cytoskeletal remodeling in contractile fibroblasts. J. Biomech. 41, 2964–2971.
Or, M., Kimmel, E., 2009. Modeling linear vibration of cell nucleus in low intensity ultrasound field. Ultrasound Med. Biol. 35, 1015–1025.
Paierowski, J.D., Dahl, K.N., Zhong, F.L., Sammak, P.J., et al., 2007. Physical plasticity of the nucleus in stem cell differentiation. Proc. Natl. Acad. Sci. U.S.A. 104, 15619–15624.
Pan, Y., Yoon, S., Zhu, L., Wang, Y., 2018. Acoustic mechanogenetics. Curr. Opin. Biomed. Eng. 7, 64–70.
Peng, X., He, W., Xin, F., Genin, G.M., Lu, T.J., 2020. The acoustic radiation force of a focused ultrasound beam on a suspended eukaryotic cell. Ultrasonics 108, 106205.
Pogoda, K., Chin, L.K., Georges, P.C., Byfield, F.R.J., et al., 2014. Compression stiffening of brain and its effect on mechanosensing by glioma cells. New J. Phys. 16, 075002.
Prisby, R.D., Lafage-Proust, M.H., Malaval, L., Belli, A., 2008. Effects of whole body vibration on the skeleton and other organ systems in man and animal models: what we know and what we need to know. Res. Rev. 2008 (7), 319–329.
Qin, Y., Li, Y., Zhang, L.Y., Xu, G.K., 2020. Stochastic fluctuation-induced cell polarization on elastic substrates: a cytoskeleton-based mechanical model. J. Mech. Phys. Solids 137, 103872.
Ranek, L., Keiding, N., Jensen, S.T., 1975. A morphometric study of normal human liver cell nuclei. Acta Pathol. Microbiol. Scand 83A, 467–476.
Reubinoff, B.E., Itsykson, P., Turetsky, T., Pera, M.F., et al., 2001. Neural progenitors from human embryonic stem cells. Nat. Biotechnol. 19, 1134–1140.
Reynolds, R.P., Li, Y., Garner, A., Norton, J.N., 2018. Vibration in mice: a review of comparative effects and use in translational research. Animal Models Exp. Med. 1, 116–124.
Rho, J.Y., Ashman, R.B., Turner, C.H., 1993. Young's modulus of trabecular and cortical bone material: ultrasonic and microtensile measurements. J. Biomech. 26, 111–119.
Saha, K., Keung, A.J., Irwin, E.F., Li, Y., et al., 2008. Substrate modulus directs neural stem cell behavior. Biophys. J. 95, 4426–4438.

Schibber, E., Mittelstein, D., Gharib, M., Shapiro, M., Lee, P., Ortiz, M., 2019. A dynamical model of oncotripsy by mechanical cell fatigue: selective cancer cell ablation by Low-Intensity Pulsed Ultrasound (LIPUS). P. Roy. Soc. A 476, 2236.
Schinagl, R.M., Gurskis, D., Chen, A.C., Sah, R.L., 1997. Depth-dependent confined compression modulus of full-thickness bovine articular cartilage. J. Orthop. Res. 15, 499–506.
Shakiba, D., Alisafaei, F., Savadipour, A., Rowe, R.A., Genin, G.M., 2020. The balance between actomyosin contractility and microtubule polymerization regulates hierarchical protrusions that govern efficient fibroblast-collagen interactions. ACS Nano 14.
Sinnamon, J.R., Waddell, C.B., Nik, S., Chen, E.I., Czaplinski, K., 2012. Hnrpab regulates neural development and neuron cell survival after glutamate stimulation. Rna-a Publ. Rna Soc. 18, 704–719.
Steinhauser, M.O., Schmidt, M., 2021. Destruction of cancer cells by laser-induced shock waves: recent developments in experimental treatments and multiscale computer simulations. Soft Matter 10, 4778.
Swailes, N.T., Colegrave, M., Knight, P.J., Peckham, M., 2006. Non-muscle myosins 2A and 2B drive changes in cell morphology that occur as myoblasts align and fuse. J. Cell Sci. 119, 3561–3570.
Tanaka, S.M., Li, J., Duncan, R.L., Yokota, H., Burr, D.B., Turner, C.H., 2003. Effects of broad frequency vibration on cultured osteoblasts. J. Biomech. 36, 73–80.
Theise, N., Krause, D.S. and Sharkis, S., 2003. Comment on "Little Evidence for Developmental Plasticity of Adult Hematopoietic Stem Cells". 299, 1317a.
Tirkkonen, L., Halonen, H., Hyttinen, J., Kuokkanen, et al., 2011. The effects of vibration loading on adipose stem cell number, viability and differentiation towards bone-forming cells. J. R. Soc. Interface 8, 1736–1747.
Tran, D., Girault, T., Guichard, M., Thomine, S., Sciences, Frachisse, J.M., 2021. Cellular transduction of mechanical oscillations in plants by the plasma-membrane mechanosensitive channel MSL10. Proc. Natl. Acad. Sci. U.S.A. 118, e1919402118.
Turner, C.H., Owan, I., Takano, Y., 1995. Mechanotransduction in bone: role of strain rate. Am. J. Physiol. 269, 438–442.
Tyler, W.J., 2012. The mechanobiology of brain function. Nat. Rev. Neurosci. 13, 867–878.
Uhler, C., Shivashankar, G.V., 2017. Regulation of genome organization and gene expression by nuclear mechanotransduction. Nat. Rev. Mol. Cell Bio. 18, 717.
Walpole, L.J., 1991a. A translated rigid ellipsoidal inclusion in an elastic medium. Proc. Math. Phys. Eng. Sci. 434, 571–585.
Walpole, L.J., 1991b. A rotated rigid ellipsoidal inclusion in an elastic medium. Proc. Math. Phys. Eng. Sci. 433, 179–207.
Wang, H., Abhilash, A.S., Chen, C.S., Wells, R.G., Shenoy, V.B., 2014. Long range force transmission in fibrous matrices enabled by tension-driven alignment of fibers. Biophys. J. 107, 2592–2603.
Wang, L., Zhao, Y., Ng, E., Lin, Q., 2005. A MEMS differential calorimeter for biomolecular characterization. In: 18th IEEE International Conference on Micro Electro Mechanical Systems, pp. 814–817.
Wang, N., Tytell, J.De, 2009. Mechanotransduction at a distance: mechanically coupling the extracellular matrix with the nucleus. Nat. Rev. Mol. Cell Bio. 10, 75.
Wilhelmsson, U., Bushongt, E., Price, D., Smarr, et al., 2006. Redefining the concept of reactive astrocytes as cells that remain within their unique domains upon reaction to injury. Proc. Natl. Acad. Sci. U.S.A. 103, 17513–17518.
Wood, A.K.W., Sehgal, C.M., 2015. A review of low-intensity ultrasound for cancer therapy. Ultrasound Med. Biol. 41, 905–928.
Yeh, W.C., Li, P.C., Jeng, Y.M., Hsu, H.C., et al., 2002. Elastic modulus measurements of human liver and correlation with pathology. Ultrasound Med 28, 467–474.
Yi, E., Sato, S., Takahashi, A., Parameswaran, H., et al., 2016. Mechanical forces accelerate collagen digestion by bacterial collagenase in lung tissue strips. Front. Physiol. 7.
Zeng, Y., Ai, K.Y., Teo, S.K., Chiam, K.H., 2012. A three-dimensional random network model of the cytoskeleton and its role in mechanotransduction and nucleus deformation. Biomech. Model Mechan. 11, 49–59.
Zhou, L.H., Liu, S.B., Wang, P.F., Lu, T.J., et al., 2016. The Arabidopsis trichome is an active mechanosensory switch. Plant Cell Environ 611.